Hindawi
Journal of Spectroscopy
Volume 2018, Article ID 6260458, 7 pages
https://doi.org/10.1155/2018/6260458

Research Article

Detailed Spectroscopic and Structural Analysis of TiO_2/WO_3 Composite Semiconductors

Biborka Boga,[1] István Székely,[2,3] Zsolt Pap,[2,3,4] Lucian Baia ,[2,3] and Monica Baia [2,3]

[1] *Faculty of Chemistry and Chemical Engineering, Babeş-Bolyai University, Arany János 11, Cluj-Napoca 400028, Romania*
[2] *Nanostructured Materials and Bio-Nano-Interfaces Center, Institute for Interdisciplinary Research on Bio-Nano-Sciences, Treboniu Laurian 42, Cluj-Napoca 400271, Romania*
[3] *Faculty of Physics, Babeş-Bolyai University, Mihail Kogălniceanu 1, Cluj-Napoca 400084, Romania*
[4] *Institute of Environmental Science and Technology, Tisza Lajos krt. 103, Szeged 6720, Hungary*

Correspondence should be addressed to Lucian Baia; lucian.baia@phys.ubbcluj.ro

Received 15 March 2018; Accepted 4 September 2018; Published 2 October 2018

Academic Editor: Vincenza Crupi

Copyright © 2018 Biborka Boga et al. This is an open access article distributed under the Creative Commons Attribution License, which permits unrestricted use, distribution, and reproduction in any medium, provided the original work is properly cited.

WO_3-TiO_2 composite materials were obtained using commercial titania (Evonik Aeroxide P25) and hydrothermally crystallized WO_3. Different ratios of TiO_2/WO_3 were investigated, starting at 1 wt.% of WO_3 to 50 wt.%. The morphology of WO_3 was of the star-like type, and its structure is basically composed of monoclinic crystalline phase. All spectroscopic characteristics of the composites and their derived data (band-gap energy value, light absorption threshold, and IR specific bands) directly varied with the increase of the WO_3 content. However, the oxalic acid photodegradation achieved under UV light reached the highest yield for 24 wt.% WO_3 content, a result that was attributed to the charge separation efficiency and the surface hydrophilicity. The latter mentioned reason points out the crucial importance of the surface quality of the investigated structure in photocatalytic tests.

1. Introduction

The study of semiconductors remained in the last years a systematically investigated research topic. The implementation of nanomaterials in the industry had a major role in the blooming research of nanomaterials. One of these nanomaterials is tungsten trioxide (WO_3), a transition metal oxide with large applicability spectra that is commonly used in paints as pigment [1], in solar cells for electricity production [2, 3], and in coatings for heat production from absorbing solar energy [4], such as humidity, moisture, and gas sensors [5–7]. This oxide is also an important component in “smart windows” due to its electrochromic properties [8]. Moreover, WO_3 is used as a catalytic and photocatalytic purifier for air and water [9, 10].

WO_3 nanomaterials (nano- or microcrystals) can be synthesized via various methods, such as hydrothermal crystallization [11], solvothermal crystallization [12], chemical vapor deposition [13], atomic layer deposition [14], physical vapor deposition [15], sol-gel synthesis [16], and laser pyrolysis [17]. There is an extensive list of possibilities towards WO_3 production, but the most widely used technique is the hydrothermal crystallization because this method is relatively simple, and it is not expensive and time-consuming [18–21].

Tungsten trioxide has an interesting peculiarity; in certain cases, it can act as a charge separator [22]. Due to this feature, it is a viable component for binary composite systems, in which another metal oxide is used as an electron donor, generally TiO_2 [23] or ZnO [24], but NiO [25] was also used. The final goal of these composite systems is either to apply them as a sensor or as a photocatalyst, or even both simultaneously. Photocatalytic efficiency of WO_3 semiconductor can be enhanced if noble metals are added, WO_3/Au, WO_3/Ag, or WO_3/Pt composite systems being related to show an improved photocatalytic efficiency towards the removal of organic pollutants in comparison with commercial TiO_2 (Evonik Aeroxide P25) [26–28]. The photocatalytic activity of ternary composites based on WO_3, commercial TiO_2, and noble metals (WO_3/TiO_2/noble metals) was also intensively studied [29–31]. The most commonly used methods for the preparation of WO_3/P25 composites are the mechanical mixing or the adjustment of the semiconductors' surface charge, and in both cases, the composites photocatalytic efficiency was improved as compared to that exhibited by P25 [32, 33].

In this study, tungsten trioxide microcrystals were synthesized via hydrothermal crystallization, and their spectroscopic and structural features were investigated. Various weight percentage composites based on the synthesized WO_3 and commercial TiO_2 (Evonik Aeroxide P25) were prepared by mechanical mixing method, and the photocatalytic activity of these binary composite systems was assessed.

2. Experimental

2.1. Chemicals. The chemicals employed for the synthesis of WO_3 microcrystals were ammonium metatungstate hydrate ($(NH_4)_6H_2W_{12}O_{40}{\cdot}xH_2O$, Sigma-Aldrich, 99.99%) and hydrochloric acid (HCl, NORDIC 37%, 12 M). The photocatalytic activity was evaluated in the aqueous solution (3 mM) of oxalic acid-OA ($HO_2C\text{-}CO_2H{\cdot}2H_2O$, Sigma-Aldrich, 98%). Commercial TiO_2 (Evonik Aeroxide P25) was used for the WO_3/TiO_2 composites preparation. All chemicals were used as received without further modification or purification.

2.2. Synthesis of Star-Like WO_3 Microcrystals. 1.23 g of ammonium metatungstate hydrate (AMT) was dissolved in 20 mL of water under constant stirring. 0.84 mL (12 M) hydrochloric acid (HCl) was added to the solution which was stirred for 15 minutes at room temperature. A yellow suspension was obtained after the hydrothermal crystallization, which was carried out at 180°C for 4 hours. After the autoclave cooled down at room temperature, the product was centrifuged (3 × 15 minutes, 1600 rpm) and washed with deionized water in order to remove the impurities remained in the product. The product was dried at 70°C for 6 hours and annealed at 500°C for 30 minutes (heating rate $5^{\circ}C\cdot min^{-1}$) [34]. The WO_3-AMT abbreviation was further used to identify the WO_3 crystals synthesized from ammonium metatungstate hydrate.

2.3. The Preparation of TiO_2/WO_3 Composites. The TiO_2/WO_3 composites were obtained via mechanical mixing (3 × 5 minutes), by using the physical mixing method. 50–50, 67–33, 76–24, 90–10, and 99–1 wt.% TiO_2/WO_3 composites were prepared and investigated. According to our previous work [29], no structural or morphological changes were observed for the two components, when mixing them by using the above-described approach.

2.4. Characterization Methods. The assessment of the crystalline structure of the composite components was carried out by the means of X-Ray Diffraction (XRD) measurements. The XRD diffractograms were recorded on a Shimadzu 6000 diffractometer (Shimadzu Corporation, Kyoto, Japan), by using Cu-Kα irradiation, ($\lambda = 1.5406$ Å). The crystalline phases of the semiconductors were evaluated and the crystallites' average size was calculated by using the Scherrer equation [35], whereas the anatase/rutile ratios in P25 were evaluated by the well-known Banfield approach [36].

Diffuse reflectance spectroscopy (DRS) measurements were performed by using the JASCO-V650 spectrophotometer ($\lambda = 250 - 800$ nm) equipped with ILV-724 integration sphere. The band-gap energy of the composites system was determined using the following equation [37–39]:

$$(E) = \frac{h \cdot c}{\lambda}, \tag{1}$$

where (E) is the band-gap energy, h is Plank constant, c is the speed of light $= 3.0 \times 10^8$ m·sec^{-1}, and λ is the cut-off wavelength.

A JASCO 4100 (Jasco, Tokyo, Japan) spectrometer was used to record the IR spectra of the composites, at room temperature, in the spectral range of 400–4000 cm^{-1}, with a spectral resolution of 4 cm^{-1}. The samples were prepared in the form of KBr pellets.

The SEM micrographs were recorded by using an FEI Quanta 3D FEG scanning electron microscope operating at an accelerating voltage of 25 kV. The WO_3 nanomaterials were covered with Au to amplify the secondary electron signal, while the morphological peculiarities of the semiconductor were uncovered.

The investigation of photocatalytic performance was carried out in the presence of 2 × 60 W fluorescence UV lamps with $\lambda \approx 365$ nm emission maximum, under vigorous stirring ($C_{suspension} = 1\ g{\cdot}L^{-1}$; $V_{suspension} = 75$ mL; $C_{oxalic\ acid} = 3$ mM). The photocatalytic degradation was followed for 3 hours using high-performance liquid chromatography (HPLC). The measurements were carried out by using Merck-Hitachi type D-7000 chromatograph equipped with an L-4250 UV-Vis detector. The volume of the loop was 20 μL and the chromatography column was installed with Grom Resin ZH-type load. The eluent was 0.06% H_2SO_4 aqueous solution, and the applied flow rate was 0.8 mL·min^{-1}. The key parameters investigated here were the conversion (X) and the reaction rate.

3. Results and Discussion

3.1. Crystalline Structure and Particle Size of the Semiconductors. The first step in the investigation series was to check the quality of the composite components. From the XRD patterns (Figure 1), the crystalline phase and the mean primary particle size of the synthesized semiconductors were established. In the case of WO_3, only the monoclinic crystalline phase was detected, as it can be seen from the diffractogram. However, based on our previous work [33], one can infer that this synthesis procedure gives rise to hierarchical structures made up from fine micrometric needle crystals (30–50 nm wide and 3-4 μm long) that form a star-like shaped structure (therefore the Scherrer equation was not used). The particle size of the WO_3 stars was between 3 and 4 μm (as described in Section 3.3). Regarding the commercial TiO_2, both anatase and rutile crystalline phases were observed, the ratio between anatase and rutile was

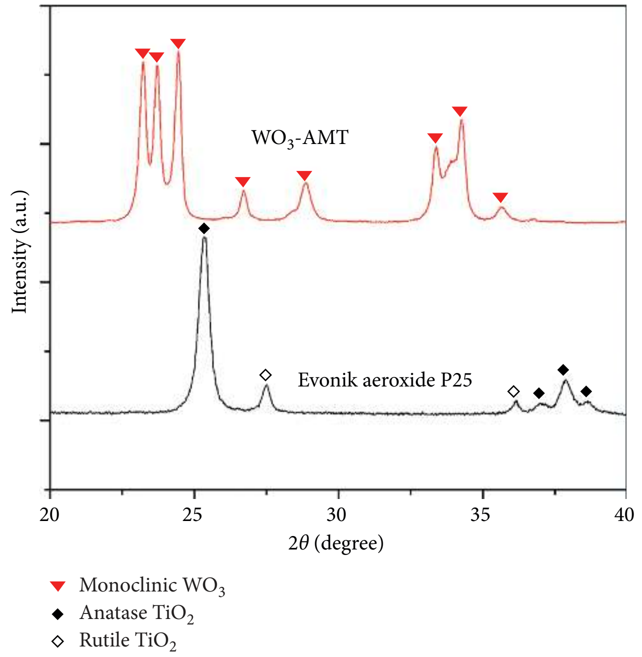

Figure 1: XRD patterns of monoclinic WO$_3$ and commercial TiO$_2$, the two components of the obtained composites.

estimated (89 : 11), and the primary calculated particle size (25–40 nm) was very close to the values reported in the literature.

3.2. Optical Properties of the Prepared Composite System. As the composite structure contains both oxides, it was crucial to investigate the optical properties of these materials (Figure 2). The band-gap energy values were determined by using the light absorption threshold method, as mentioned in Section 2.4. In the case of the WO$_3$-AMT semiconductor, the light absorption threshold was found to be around 550 nm and the calculated band-gap energy was of ≈2.25 eV, but it should be kept in mind that the band-gap energy value of the commercial TiO$_2$ is ≈3.2 eV [33]. Concerning the composites, the light absorption thresholds and the band-gap energy values were as follows: 394 nm, ≈3.14 eV (99-1 wt.% P25-WO$_3$); 414 nm, ≈2.99 eV (90-10 wt.% P25-WO$_3$); 449 nm, ≈2.76 eV (76-24 wt.% P25-WO$_3$); 447 nm, ≈2.77 eV (67-33 wt.% P25-WO$_3$); and 451 nm, ≈2.74 eV (50-50 wt.% P25-WO$_3$). The lowest band-gap energy was found for the 50-50 wt.% P25-WO$_3$ composite. One observes that the WO$_3$ amount has a significant effect on the band-gap energy value, and a very interesting fact is that even 1% of monoclinic tungsten trioxide can influence it, by slightly reducing this value by 0.06 eV. By adding 10% WO$_3$ to the composite composition, the band-gap energy was found to further decrease by 0.21 eV. By increasing the amount of WO$_3$ to 24%, the band-gap energy was lowered by 0.44 *e*V. According to these results, the 99-1% wt.% P25-WO$_3$ and 90-10% wt.% P25-WO$_3$ composites should act as photocatalysts under UV light irradiation, while the 76-24% wt.% P25-WO$_3$, 67–33% wt.% P25-WO$_3$, and 50-50% wt.% P25-WO$_3$ composites may have photocatalytic potential under visible light irradiation.

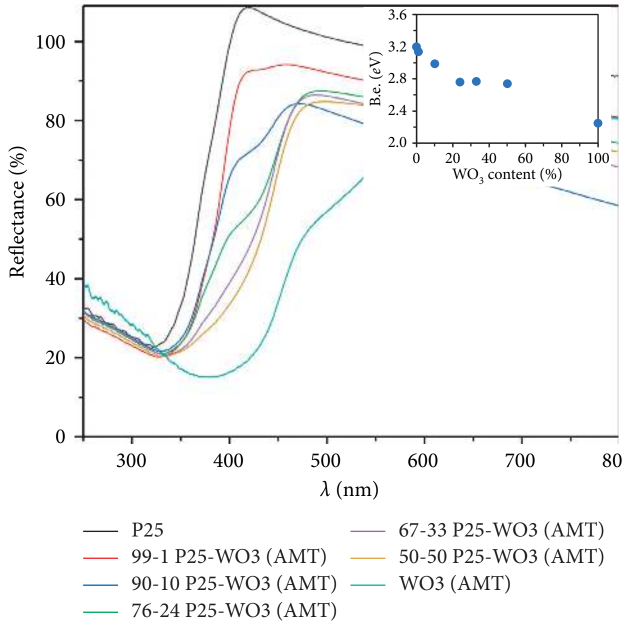

Figure 2: The reflectance spectra of the prepared WO$_3$/TiO$_2$ composites system and the band-gap energy dependence on the WO$_3$ content (inset figure).

3.3. Morphological Features of the Synthesized Semiconductor. SEM measurements revealed that the morphology of the WO$_3$ (WO$_3$-AMT) microcrystals synthesized from ammonium metatungstate hydrate was of star-like type (Figure 3). The diameter of the stars was between 3 and 4 μm, each star being constructed from microfibers of 3–4 μm length. More importantly, it was found that all the microstars showed the same structure and morphology (i.e., high monodispersity), which can reinforce all the conclusions derived from the study.

3.4. FT-IR Characterization of the Prepared Composites System. By analyzing the IR spectra (Figure 4) of the obtained composites, the specific signals of TiO$_2$ were detected without any special changing trends, excepting the alteration of some signals proportionally with the composite components' ratio. The main spectral feature associated with titania was the large band between 400 and 700 cm^{-1}, which can be attributed to the stretching vibrations of Ti-O-Ti and Ti-O bonds. In the case of WO$_3$, several specific spectral characteristics were observed, such as the ones between 600 and 1000 cm^{-1} (the most intense one being located at 931 cm^{-1}), which were assigned to different W-O-W stretching modes. The small but distinct band at 1035 cm^{-1} was given by the stretching vibration of the W = O bonds [40]. These signals involving tungsten bond vibrations were also dependent on the WO$_3$ concentration. The band at 1390 cm^{-1} was interestingly found to be given by NH$_4^+$ ions [41]. At the first view, this is rather surprising; but actually, it can be considered an expected appearance having in view that WO$_3$ was obtained by using

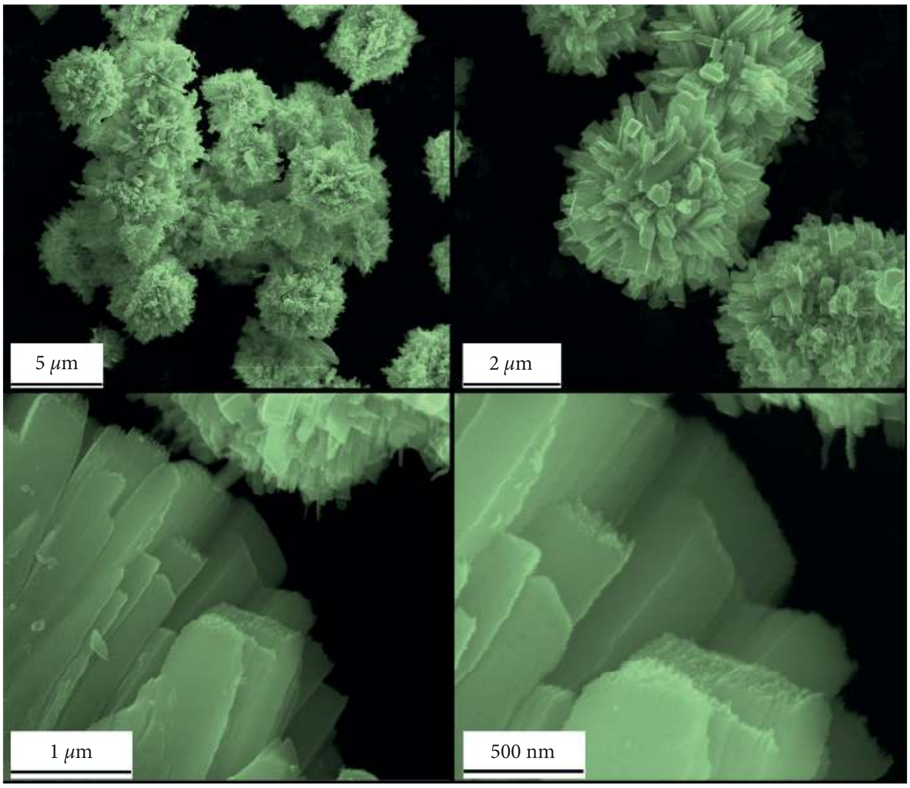

Figure 3: SEM micrographs of the WO_3-AMT semiconductors, showing the star-like shape and a fine hierarchical structure.

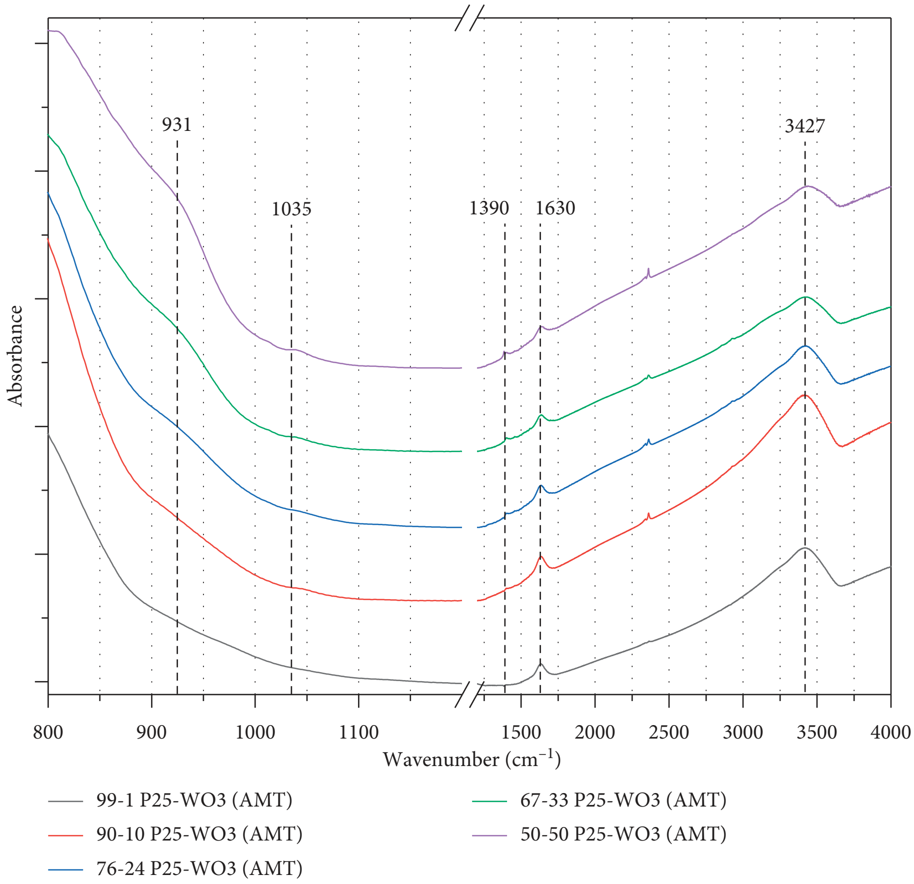

Figure 4: Infrared spectra of the prepared WO_3/TiO_2 composite system.

ammonium metatungstate. The only bands that differently changed self-dependent on the WO_3 content were those directly related to the surface hydrophilicity, namely, those at 1630 and 3427 cm^{-1} assigned to OH vibrations. These bands exhibit a relatively high intensity for the samples with ≥24 wt.% WO_3 and a slow decrease of it for smaller WO_3 content. This result points out the high water affinity of 90-10 wt.% P25-WO_3 and 76-24 wt.% P25-WO_3, which could have on impact on the photoactivity of these materials.

3.5. Photocatalytic Activity. The evaluation of the photocatalytic performance was carried out by analyzing the oxalic acid degradation curves, which provide qualitative and quantitative information (Figure 5). The photocatalytic performance was quantitatively described by using the conversion values (X).

No photocatalytic activity was observed when bare WO_3 and 50-50 wt.% TiO_2/WO_3 were used as photocatalysts in 3 mM oxalic acid solution. This photocatalytic inefficiency of bare WO_3 could be due to the WO_3 particles dimension, which is relatively high (3–4 μm). In the case of 50-50 wt.% TiO_2/WO_3 composite, the reason could be the screening effect of the WO_3 crystals on the TiO_2 particles so that the system had a deficiency being activated under UV light irradiation. In this case, the generation of charge carriers was decreased, and consequently, the photocatalytic activity was low in the composites with high WO_3 content. Only 28% of oxalic acid was removed using the 67-33 wt.% TiO_2/WO_3 composite system in contrast to 76-24 wt.% TiO_2/WO_3 system, where 99% conversion was achieved. 68% conversion was obtained in the case of 90-10 wt.% TiO_2/WO_3 composites and 95% conversion rate was observed for the 99-1 wt.% TiO_2/WO_3 composites. The reference catalyst (commercial TiO_2) degraded 73.3 wt.% of oxalic acid.

The most efficient composite for oxalic acid degradation was the 76-24 wt.% TiO_2/WO_3 system because the recombination process was inhibited successfully so that the separation of the charge carriers was the most efficient in the case of this sample. The first five points were taken into consideration for the calculation of the initial reaction rates. The concentration changes of oxalic acid (at 0, 15, 30, 45, and 60 min) were plotted versus time to determine the initial reaction rate (r_i) values. The linearization of these two parameters and its slope gave the initial reaction rate values. The initial reaction rate of the bare WO_3 and of 50-50 wt.% TiO_2-WO_3 composites were null because these systems were not photoactive. In the other cases, the reaction rate was 5.80 $mM{\cdot}s^{-1}{\cdot}10^{-3}$ (67-33%), 22.10 $mM{\cdot}s^{-1}{\cdot}10^{-3}$ (76-24%), 12.90 $mM{\cdot}s^{-1}{\cdot}10^{-3}$ (90-10%), 11.40 $mM{\cdot}s^{-1}{\cdot}10^{-3}$ (99-1%), and 12.7 $mM{\cdot}s^{-1}{\cdot}10^{-3}$ (in the case of commercial TiO_2). The conversion, initial reaction rate, and band-gap energy values are summarized in Table 1.

All the activity-related parameters clearly show that it must be a specific parameter responsible for the high photoactivity. The band-gap energy values of the composites can be eliminated as the main reason because it is a parameter that varied concomitantly with the WO_3 content. As no structural and morphological changes occurred during the composite preparation, other approaches should be exploited. Firstly, an analog case can be involved, in which a similar phenomenon was explained [29]. As the amount of WO_3 increases, so does the charge separation efficiency in the composites. However, after a specific concentration of WO_3, this was detrimental, because the WO_3 itself is not photoactive. This means that increasing too much the ratio of a charge separator (without self-activity), a lowering of the overall photoactivity occurs. However, this approach may be not sufficient alone. The intensity of the IR bands at 1630 cm^{-1} and 3427 cm^{-1} showed nearly the same trend as the photoactivity. This means that the photocatalytic degradation is in direct relationship with the hydrophilicity of the photocatalyst (a fact well-known for TiO_2 [42]), which was confirmed here for the first time in case of TiO_2-WO_3 composites.

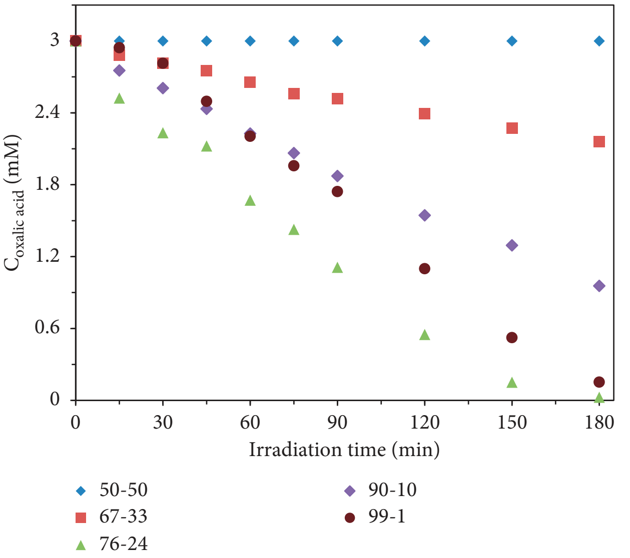

Figure 5: Photodegradation of 3 mM oxalic acid using under UV light irradiation in the presence of 50-50, 67-33, 76-24, 90-10, and 99-1 wt.% TiO_2/WO_3 composites.

Table 1: Summary of the photocatalytic properties for the various composite system and reference catalysts.

Samples	X—conversion (%) (after 3 hours)	r_i $(mM{\cdot}second^{-1}){\cdot}10^{-3}$	Band-gap energy value (eV)
WO_3 (AMT)	0.0	0.0	2.25
P25	73.3	12.7	3.20
50% P25-50% WO_3 (AMT)	0.0	0.0	2.74
67% P25-33% WO_3 (AMT)	28.0	05.8	2.77
76% P25-24% WO_3 (AMT)	**99.0**	**22.1**	**2.76**
90% P25-10% WO_3 (AMT)	68.0	12.9	2.99
99% P25-1% WO_3 (AMT)	95.0	11.4	3.14

4. Conclusions

In the herein presented study, WO_3-TiO_2 composites with different TiO_2/WO_3 ratios (1 wt.% of WO_3 to 50 wt.%) were obtained by using commercial titania (Evonik Aeroxide P25) and hydrothermally crystallized WO_3. The morphology of the synthesized hierarchical WO_3 semiconductors was star-like shaped with a diameter between 3 and 4 μm, and WO_3's determined crystal phase was monoclinic. The present study proves that WO_3 microcrystals of relatively large dimension, without photoactivity, can improve the photocatalytic efficiency of the commercial TiO_2, acting as a charge separator. The band-gap energy values of the composites were found to be dependent on the WO_3 content as well, but no correlation was established with the photoactivity.

The 76-24 wt.% TiO_2/WO_3 composite system has shown the highest photocatalytic activity, reaching a conversion rate of 99%. Also, this sample and the one with 10 wt.% of WO_3 exhibited the most intense water affinity as revealed by the IR bands assigned to water vibrations, showing a clear correlation between these structural entities and photoactivity.

The obtained results from this study also suggest that these composites system could be used as efficient photocatalysts for other pollutants removal (methyl orange and salicylic acid), gas sensors, and sensors for detection of organic pollutants containing the carboxylic functional group or could be even used for ternary WO_3/TiO_2/noble metal composites.

Data Availability

All the data shown throughout the five figures and one table used to support the findings of this study are included within the article.

Conflicts of Interest

The mentioned received funding did not lead to any conflicts of interest regarding the publication of this manuscript. Furthermore, the authors do not have any other conflicts of interest, concerning the present work.

Authors' Contributions

Biborka Boga and István Székely contributed equally to this work.

Acknowledgments

Biborka Boga would like to thank the Hungarian Ministry of Economic and Foreign Affairs for the scholarship "Márton Áron" Programme for Gifted Youngsters. István Székely acknowledges the funding provided by the Collegium Talentum scholarship supported by the Sapientia Hungariae Foundation. Biborka Boga, István Székely, and Zsolt Pap would like to express their gratitude towards the "RING 2017," EFOP-3.6.2-16-2017-00010 project, funded by the European Union and the Government of Hungary. In addition, the authors would like to thank Dr. Klára Magyari for recording the IR spectra and Zsejke-Réka Tóth for the photocatalytic tests.

References

[1] P. Patnaik, *Handbook of Inorganic Chemicals*, McGraw-Hill, New York, NY, USA, 2003.

[2] M. Gómez, J. Lu, E. Olsson, A. Hagfeldt, and C. Granqvist, "High efficiency dye-sensitized nanocrystalline solar cells based on sputter deposited Ti oxide films," *Solar Energy Materials and Solar Cells*, vol. 64, no. 1, pp. 385–392, 2000.

[3] T. Lindgren, J. M. Mwabora, E. Avendano et al., "Photoelectrochemical and optical properties of nitrogen doped titanium dioxide films prepared by reactive DC magnetron sputtering," *Journal of Physical Chemistry B*, vol. 107, no. 24, pp. 5709–5716, 2003.

[4] P. C. Lansåker, P. Petersson, G. A. Niklasson, and C. G. Granqvist, "Thin sputter deposited gold films on In_2O_3:Sn, SnO_2:In, TiO_2 and glass: optical, electrical and structural effects," *Solar Energy Materials and Solar Cells*, vol. 117, pp. 462–470, 2013.

[5] A. Tripathi, V. Tripathi, N. K. Pandey, and K. Tiwari, "Resistive type moisture sensor based on WO_3 nanomaterial," *Sensors and Transducers*, vol. 143, pp. 152–161, 2012.

[6] J. L. Solis, A. Hoel, L. B. Kish, C. G. Granqvist, S. Saukko, and V. Lantto, "Gas-sensing properties of nanocrystalline WO_3 films made by advanced reactive gas deposition," *Journal of the American Ceramic Society*, vol. 84, no. 7, pp. 1504–1508, 2001.

[7] K. Galatsis, Y. X. Li, W. Wlodarski et al., "Comparison of single and binary oxide MoO_3, TiO_2 and WO_3 sol-gel gas sensors," *Sensors and Actuators B: Chemical*, vol. 83, no. 1–3, pp. 276–280, 2002.

[8] E. Lassner and W. Schubert, *Tungsten: properties, chemistry, technology of the elements, alloys, and chemical compounds*, Springer, Berlin, Germany, 1999.

[9] A. Amoozadeh and S. Rahmani, "Nano-WO3-supported sulfonic acid: New, efficient and high reusable heterogeneous nano catalyst," *Journal of Molecular Catalysis A: Chemical*, vol. 396, pp. 96–107, 2015.

[10] K. Sayama, H. Hayashi, T. Arai, M. Yanagida, T. Gunji, and H. Sugihara, "Highly active WO_3 semiconductor photocatalyst prepared from amorphous peroxo-tungstic acid for the degradation of various organic compounds," *Applied Catalysis B: Environmental*, vol. 94, no. 1-2, pp. 150–157, 2010.

[11] S. Cao, C. Zhao, T. Han, and L. Peng, "Hydrothermal synthesis, characterization and gas sensing properties of the WO3 nanofibers," *Materials Letters*, vol. 169, pp. 17–20, 2016.

[12] Z. Wang, M. Hu, and Y. Qin, "Solvothermal synthesis of WO_3 nanocrystals with nanosheet and nanorod morphologies and the gas-sensing properties," *Materials Letters*, vol. 171, pp. 146–149, 2016.

[13] N. Shankar, M. F. Yu, S. P. Vanka, and N. G. Glumac, "Synthesis of tungsten oxide (WO_3) nanorods using carbon nanotubes as templates by hot filament chemical vapor deposition," *Materials Letters*, vol. 60, no. 6, pp. 771–774, 2006.

[14] I. M. Szilágyi, E. Santala, M. Heikkilä et al., "Photocatalytic properties of WO_3/TiO_2 core/shell nanofibers prepared by electrospinning and atomic layer deposition," *Chemical Vapor Deposition*, vol. 19, no. 4–6, pp. 149–155, 2013.

[15] Y. B. Li, Y. Bando, D. Golberg, and K. Kurashima, "WO3 nanorods/nanobelts synthesized via physical vapor deposition process," *Chemical Physics Letters*, vol. 367, no. 1-2, pp. 214–218, 2003.

[16] T. Yang, Y. Zhang, and C. Li, "Large scale production of spherical WO_3 powder with ultrasonic spray pyrolysis assisted by sol–gel method for hydrogen detection," *Ceramics International*, vol. 40, no. 1, pp. 1765–1769, 2014.

[17] M. Govender, L. Shikwambana, B. W. Mwakikunga, E. Sideras-Haddad, R. M. Erasmus, and A. Forbes, "Esopen access formation of tungsten oxide nanostructures by laser pyrolysis: Stars, fibers, and spheres," *Nanoscale Research Letters*, vol. 6, no. 1, p. 166, 2011.

[18] M. Ahmadi, R. Younesi, and M. J. F. Guinel, "Synthesis of tungsten oxide nanoparticles using a hydrothermal method at ambient pressure," *Journal of Materials Research*, vol. 29, no. 13, pp. 1424–1430, 2014.

[19] S. Bai, K. Zhang, R. Luo, D. Li, A. Chen, and C.C. Liu, "Low-temperature hydrothermal synthesis of WO_3 nanorods and their sensing properties for NO_2," *Journal of Materials Chemistry*, vol. 22, no. 25, p. 12643, 2012.

[20] D. J. Ham, A. Phuruangrat, S. Thongtem, and J. S. Lee, "Hydrothermal synthesis of monoclinic WO3 nanoplates and nanorods used as an electrocatalyst for hydrogen evolution reactions from water," *Chemical Engineering Journal*, vol. 165, no. 1, pp. 365–369, 2010.

[21] S. S. Shendage, V. L. Patil, S. A. Vanalakar et al., "Sensitive and selective $\{NO_2\}$ gas sensor based on $\{WO_3\}$ nanoplates," *Sensors and Actuators B: Chemica*, vol. 240, pp. 426–433, 2017.

[22] K. Tennakone, O. A. Ileperuma, J. M. S. Bandara, and W. C. B. Kiridena, "TiO_2 and WO_3 semiconductor particles in contact: photochemical reduction of WO_3 to the non-stoichiometric blue form," *Semiconductor Science and Technology*, vol. 7, no. 3, pp. 423-424, 1992.

[23] B. Tryba, M. Piszcz, and A. W. Morawski, "Photocatalytic Activity of TiO_2/WO_3 Composites," *International Journal of Photoenergy*, vol. 2009, Article ID 297319, 7 pages, 2009.

[24] J. Xie, Z. Zhou, Y. Lian et al., "Simple preparation of WO_3-ZnO composites with UV-Vis photocatalytic activity and energy storage ability," *Ceramics International*, vol. 40, no. 8, pp. 12519–12524, 2014.

[25] M. Bao, Y. Chen, F. Li et al., "Plate-like p–n heterogeneous NiO/WO_3 nanocomposites for high-performance room temperature NO_2 sensors," *Nanoscale*, vol. 6, no. 8, p. 4063, 2014.

[26] D. P. Depuccio, P. Botella, B. O'Rourke, and C. C. Landry, "Degradation of methylene blue using porous WO_3, SiO_2-WO_3, and their Au-loaded analogs: Adsorption and photocatalytic studies," *ACS Applied Materials and Interfaces*, vol. 7, no. 3, pp. 1987–1996, 2015.

[27] W. Zhu, J. Liu, S. Yu, Y. Zhou, and X. Yan, "Ag loaded WO_3 nanoplates for efficient photocatalytic degradation of sulfanilamide and their bactericidal effect under visible light irradiation," *Journal of Hazardous Materials*, vol. 318, pp. 407–416, 2016.

[28] Z. Wen, W. Wu, Z. Liu, H. Zhang, J. Li, and J. Chen, "Ultrahigh-efficiency photocatalysts based on mesoporous Pt–WO_3 nanohybrids," *Physical Chemistry Chemical Physics*, vol. 15, no. 18, p. 6773, 2013.

[29] É. Karácsonyi, L. Baia, A. Dombi et al., "The photocatalytic activity of TiO_2/WO_3/noble metal (Au or Pt) nanoarchitectures obtained by selective photodeposition," *Catalysis Today*, vol. 208, pp. 19–27, 2013.

[30] M. Rusu, M. Baia, Zs. Pap, V. Danciu, and L. Baia, "Structural investigations of TiO_2-WO_3-Au porous composites," *Journal of Molecular Structure*, vol. 1073, pp. 150–156, 2014.

[31] G. Kovács, L. Baia, A. Vulpoi et al., "TiO_2/WO_3/Au nanoarchitectures' photocatalytic activity, "from degradation intermediates to catalysts' structural peculiarities", part I: Aeroxide P25 based composites," *Applied Catalysis B: Environmental*, vol. 147, pp. 508–517, 2014.

[32] L. Baia, E. Orbán, S. Fodor et al., "Preparation of TiO_2/WO_3 composite photocatalysts by the adjustment of the semiconductors' surface charge," *Materials Science in Semiconductor Processing*, vol. 42, pp. 66–71, 2016.

[33] I. Székely, G. Kovács, L. Baia, V. Danciu, and Zs. Pap, "Synthesis of shape-tailored WO_3 micro-/nanocrystals and the photocatalytic activity of WO_3/TiO_2 composites," *Materials*, vol. 9, no. 4, p. 258, 2016.

[34] S. K. Biswas and J. O. Baeg, "A facile one-step synthesis of single crystalline hierarchical WO3with enhanced activity for photoelectrochemical solar water oxidation," *International Journal of Hydrogen Energy*, vol. 38, no. 8, pp. 3177–3188, 2013.

[35] R. Jenkins and R. Snyder, *Introduction to Powder Diffractometry*, John Wiley & Sons, New York, NY,USA, 1996.

[36] H. Zhang and J. F. Banfield, "Understanding polymorphic phase transformation behavior during growth of nanocrystalline aggregates: insights from TiO_2," *Journal of Physical Chemistry B*, vol. 104, no. 15, pp. 3481–3487, 2000.

[37] M. R. Hoffmann, S. T. Martin, W. Choi, and D. W. Bahnemann, "Environmental Applications of Semiconductor Photocatalysis," *Chemical Reviews*, vol. 95, no. 1, pp. 69–96, 1995.

[38] S. S. Srinivasan, N. Kislov, J. Wade, M. T. Smith, E. K. Stefanakos, and Y. Goswami, "Mechanochemical synthesis, structural characterization and visible light photocatalysis of $TiO_2/ZnFe_2O_4$ nanocomposites," in *Proceedings of Symposium Materials Research Society*, December 2005.

[39] S. S. Srinivasan, J. Wade, and E. K. Stefanakos, "Synthesis and Characterization of Photocatalytic TiO_2-$ZnFe_2O_4$ Nanoparticles," *Journal of Nanomaterials*, vol. 2006, Article ID 45712, 4 pages, 2006.

[40] H. I. S. Nogueira, A. M. V. Cavaleiro, J. Rocha, T. Trindade, and J. D. P. De Jesus, "Synthesis and characterization of tungsten trioxide powders prepared from tungstic acids," *Materials Research Bulletin*, vol. 39, no. 4-5, pp. 683–693, 2004.

[41] J. Westerhaus, *Infrared Spectra of the Ammonium Ion in Crystals*, Royal Society of Chemistry, Cambridge, UK, 1981.

[42] Zs. Pap, V. Danciu, Zs. Cegléd et al., "The influence of rapid heat treatment in still air on the photocatalytic activity of titania photocatalysts for phenol and monuron degradation," *Applied Catalysis B: Environmental*, vol. 101, pp. 461–470, 2011.

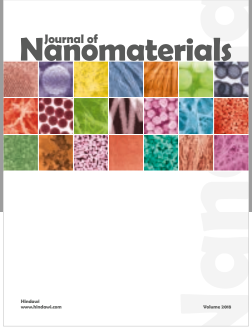

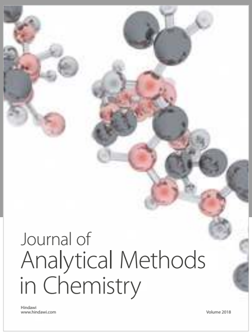

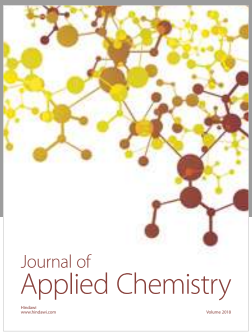

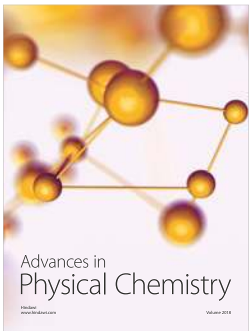

Hindawi

Submit your manuscripts at
www.hindawi.com